Available online at www.sciencedirect.com
ScienceDirect
Journal of Crystal Growth 310 (2008) 2485–2492
JOURNAL OF CRYSTAL GROWTH
www.elsevier.com/locate/jcrysgro

Site-specific growth of ZnO nanowires from patterned Zn via compatible semiconductor processing

J.B.K. Law[a,b], C.B. Boothroyd[b], J.T.L. Thong[a,*]

[a]*Department of Electrical and Computer Engineering, National University of Singapore, 4 Engineering Drive 3, 117576, Singapore*
[b]*Institute of Materials Research and Engineering, 3 Research Link, 117602, Singapore*

Received 15 October 2007; received in revised form 7 January 2008; accepted 13 January 2008
Communicated by T.F. Kuech
Available online 19 January 2008

Abstract

An alternative method for site-selective growth of ZnO nanowires without the use of an Au catalyst or a ZnO thin-film seed layer is presented. Using conventional lithography and metallization semiconductor processing steps, regions for selective nanowire growth are defined using Zn, which acts as a self-catalyst for subsequent ZnO nanowire growth via a simple thermal oxidation process. Scanning electron microscopy, transmission electron microscopy and X-ray diffraction reveal that the nanowires grown by this technique are single-crystalline wurtzite ZnO. Room temperature photoluminescence exhibits strong ultraviolet emission from these nanowires, indicating good optical properties. A series of experiments was conducted to elucidate the unique growth behavior of these nanowires directly from the Zn grains and a growth model is proposed.

PACS: 81.07.−b; 81.16.Dn; 81.16.−c

Keywords: A1. Crystal structure; A1. Growth model; A1. Nanostructures; A2. Thermal oxidation; A3. Patterned growth; B1. ZnO nanowires

1. Introduction

Zinc oxide (ZnO) nanowires have attracted extensive research interest as one-dimensional nanostructures in recent years due to their many attractive electrical, optical, and chemical properties [1,2]. Currently, a variety of techniques have been used for the successful synthesis of ZnO nanowires. These can generally be classified into vapor–liquid–solid (VLS) techniques, thermal-evaporation and condensation by vapor–solid (VS) techniques, as well as solution-based growth techniques [3–6]. Though excellent results have been obtained so far in the controlled synthesis of nanowire geometry and properties [1–6], for practical device applications, it is necessary to develop techniques that allow these nanowires to be grown at specific locations on a substrate. Currently, most of the reported work on such selective growth on substrates employs the gold (Au) catalyst-assisted VLS technique in which Au catalyst dots or films are used to seed the patterned growth of the ZnO nanowires [4,7–10]. Nevertheless, there are a few issues concerning the use of Au for patterned nanowire synthesis. Firstly, Au particles may be embedded at the tip of the nanowire due to the nanowire's intrinsic growth nature, and this might affect the properties of these nanowires as well as degrade the performance of devices made with these nanowires. Secondly, Au may be a source of contamination that is detrimental to conventional silicon (Si) fabrication environments (for example, Au atoms can act as efficient recombination centers in Si) [11]. Thus, it is desirable to develop techniques for patterned synthesis of ZnO nanowires, which avoid the use of an Au metal catalyst. Both the thermal-evaporation and condensation VS growth and the solution-based technique of nanowire growth avoid the use of Au catalyst. However, it is widely known that these techniques provide less control over the spatial location for nanowire growth [4]. Recently, Conley et al. and Cross et al. demonstrated

*Corresponding author. Tel.: +65 6516 2270; fax: +65 6516 7912.
E-mail address: elettl@nus.edu.sg (J.T.L. Thong).

0022-0248/$ - see front matter © 2008 Elsevier B.V. All rights reserved.
doi:10.1016/j.jcrysgro.2008.01.012

selective patterned growth of ZnO nanowires by utilizing a ZnO thin-film seed layer grown using the VS technique [11] and the solution-based technique [12], respectively. However, costly and elaborate processing to deposit the ZnO thin film layer (e.g. by atomic layer deposition) is needed.

Furthermore, in most work on site-specific growth of ZnO nanowires, the nanostructures are aligned vertically with respect to the substrate through an epitaxial relationship with the underlayer. Although integration of vertically aligned geometries for device applications has been demonstrated [4,13,14], such integration processes are not in-line with conventional planar integrated circuit (IC) manufacturing. On the other hand, currently, most planar ZnO nanodevices are fabricated by using the post-growth "pick and place" technique. Such a technique is tedious and time consuming. Furthermore, it is only suitable for one-off device fabrication and only allows arbitrary positioning of individual nanowire laterally on a substrate [1–3]. If nanostructures can be synthesized with lateral geometries and at specific locations on a substrate, integration of such planar nanostructures into devices would be much simpler and cost-effective by leveraging on the existing mature Si planar device platform. The synthesis of ZnO nanowires with a laterally aligned geometry is recently demonstrated by Kim et al. [15] and Fan et al. [16] using the VS technique by evaporation of the Zn source followed by random deposition of Zn grains at a cooler region of the substrate with differing thermal oxidation conditions. However, site-selective growth is not demonstrated in these reports.

In this work, we demonstrate an alternative method for site-selective patterned growth of ZnO nanowires without the use of an Au catalyst or a ZnO thin-film seed layer. Instead, we make use of the conventional semiconductor processing steps of lithography and metallization. Regions for selective nanowire growth are defined using Zn metal grains, which act as a self-catalyst for subsequent ZnO nanowire growth via a simple thermal oxidation process. Characterization of the morphology, microstructure, and optical properties of these nanowires was carried out. A series of experiments was conducted in order to elucidate the unique growth behavior of these nanowires, which grow laterally from the edges of the Zn grains, and a growth model is proposed.

2. Experimental details

Fig. 1 shows a typical process flow for the patterned synthesis of ZnO nanowires. Starting with a silicon nitride (Si_3N_4) insulated silicon (Si) substrate, lithography is performed to define desired regions for nanowire growth using a resist (Fig. 1a). Next, Zn metal is evaporated over the resist using a thermal vacuum evaporator with an Ar plasma cleaning function (BOC Edwards, Auto 306 Vacuum Evaporator). The sample can either be subjected to Ar plasma sputtering for 10 s or can be coated with a thin layer (4 nm) of predeposited gold to promote Zn metal

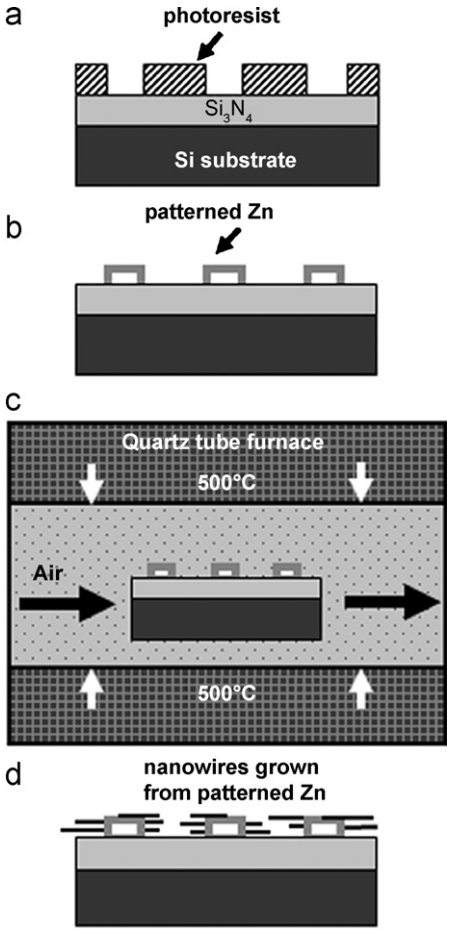

Fig. 1. Diagram illustrating site-specific growth of ZnO nanowires from patterned Zn on a Si_3N_4 insulated Si substrate.

deposition. The 100 nm of Zn metal is thermally evaporated using Zn wire (99.9999% purity) as the source material at a vacuum pressure of 3×10^{-6} mbar. After metallization, the sample undergoes lift-off in acetone to define the patterned regions (Fig. 1b). Next, the sample is placed in the middle of a quartz tube furnace and subjected to thermal oxidation in air at atmospheric pressure and a growth temperature of 500 °C over a duration of 10 min before cooling down to room temperature (Fig. 1c). Nanowires grow from the patterned regions after thermal oxidation (Fig. 1d).

An important factor that distinguishes our growth technique from similar technique in Refs. [15,16] is the ability to grow ZnO nanowires at site-selective location on a silicon substrate. This is achieved by selective deposition of Zn grains on predefined areas on an insulating substrate by lithography, which contrasts with those in Refs. [15,16] showing randomly deposited Zn grains. However, to deposit Zn grains onto insulating amorphous surfaces is theoretically not feasible. An insulating layer is required for the fabrication of devices on a silicon substrate. In theory, it is difficult to deposit Zn onto amorphous surfaces (e.g. Si_3N_4): in order for material A to be deposited onto a substrate B, one must satisfy the condition $\gamma_B > \gamma_A + \gamma^*$ [17],

where γ_A is the surface energy of the material to be deposited, γ_B is the surface energy of the substrate material, and γ^* is the interfacial energy. This condition cannot be met for Zn deposition onto a silicon nitride surface since the surface energy of Zn ($\gamma_A \sim 1\,J/m^2$) [18] is higher than that of Si_3N_4 ($\gamma_B \sim 0.1\,J/m^2$) [19], while the interfacial energy γ^* can be considered negligible as the two materials are mutually insoluble. To overcome this challenge, we propose two possible methods. The first method uses a thin layer of Au (4 nm) deposited prior to Zn evaporation. Gold is known to act as a nucleation site for Zn vapor to form a deposit as has been demonstrated in Refs. [20,21]. However, Au is not welcomed in conventional semiconductor fabrication. In an alternative method, we subject the surface of the sample to plasma sputtering in Ar for a short duration (~10 s). Zn can also be deposited directly onto the nitride surface without the intervening Au layer. It is a well-known fact that plasma sputtering roughens surfaces, and a rough surface is known to act as a preferred nucleation site for Zn metal vapor deposition [21,22]. It is noted that our two proposed methods for Zn deposition produce similar Zn grains and ZnO nanowires in terms of morphology and orientation from scanning electron microscopy (SEM) and transmission electron microscopy (TEM) investigations.

Field emission SEM (FESEM, Phillips XL30 FEG), TEM (Phillips CM300), X-ray diffraction (XRD, Bruker GADDS with Cu Kα radiation) and room temperature photoluminescence (PL) spectroscopy (Renishaw 2000 PL system with a 325 nm HeCd laser as the excitation source) were employed to investigate the morphology, microstructure, and optical properties of these nanowires. To elucidate the nanowires unique growth behavior, detailed characterization was carried out starting from the deposited Zn grains (which seed the nanowire growth) to the ZnO nanowires using FESEM and TEM.

3. Results and discussion

3.1. Selective growth of ZnO nanowires from patterned Zn

SEM images of arrays consisting of 2 μm diameter circles and 2×2 μm squares of patterned Zn to illustrate the selective patterning are shown in Figs. 2a and b. The Zn is deposited by Ar sputtering pretreatment method. A typical patterned Zn region consists of many randomly placed Zn grains whose diameters range from 150 to 250 nm. The results of selective growth of nanowires from different patterned Zn regions after 10 min of thermal oxidation are shown in the SEM images of Figs. 2c and d. The typical nanowire length is around 500 nm. Longer nanowires (with lengths of about 1.5 μm) are grown when the thermal oxidation duration is increased to 1 h. In addition, Fig. 2e illustrates the scalable capability of this technique: by using a patterned array, a large network of interconnected nanowires can be readily achieved using a single *in situ* growth process. The inset of Fig. 2e shows the *I–V* measurement across both ends of a patterned array measuring 125×45 μm, indicating ohmic characteristics. Such large-scale networks of nanowires are very attractive candidates as gas/chemical sensors due to their large surface-to-volume ratio.

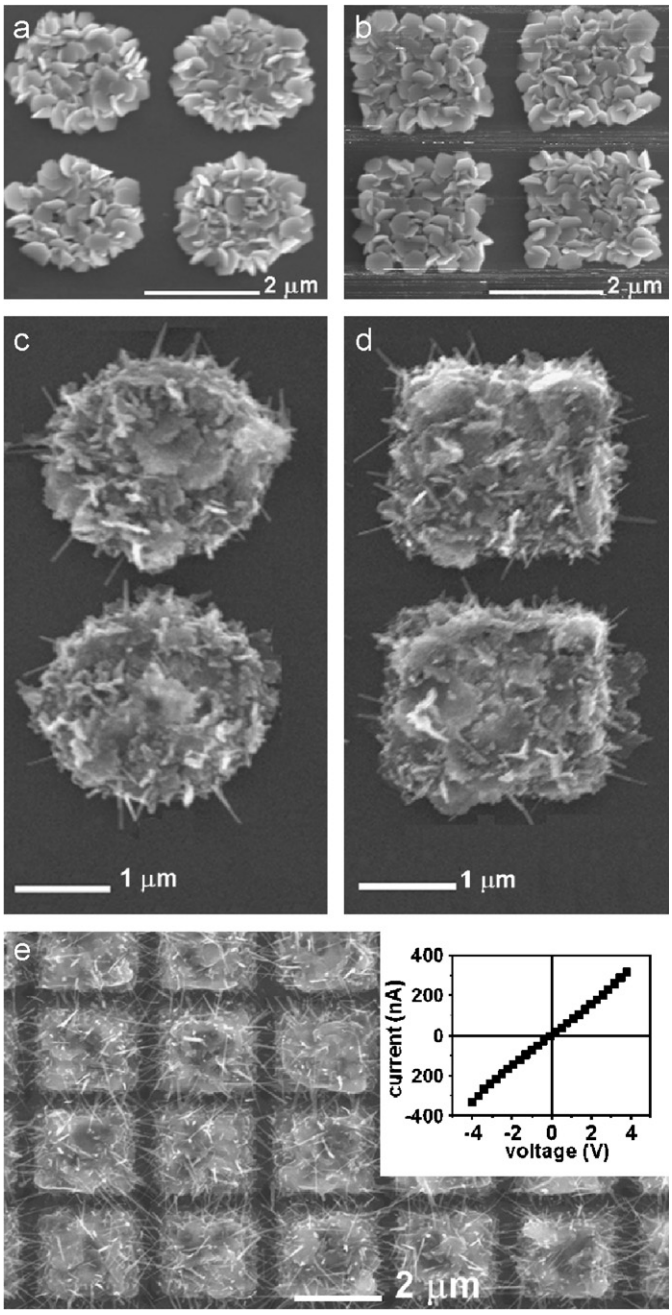

Fig. 2. SEM images showing: (a) and (b) different types of patterned Zn regions, (c) and (d) selective growth of nanowires from the patterned Zn regions, and (e) network of interconnected nanowires formed from a patterned array. Inset of (e) shows the *I–V* curve measured across the patterned array showing ohmic characteristics.

3.2. Characterization

The as-grown nanowires were analyzed in an X-ray diffractometer and were found to consist of hexagonal ZnO

(space group $P6_3mc$; $a = 0.3242$ nm, $c = 0.5188$ nm) with some remaining Zn (Fig. 3). Comparing with similar growth technique in Refs. [15,16], Zn traces is also observed by Fan et al. [15] while Kim et al. [16] observed a full conversion to ZnO from Zn seeds. This variation could be due to a difference in the oxidation time needed for full conversion of Zn to ZnO in both cases. In our case, we managed to fully convert Zn to ZnO with a longer oxidation time (~3 h).

The optical properties of these ZnO nanowires were investigated by room temperature PL. The PL spectrum (Fig. 4) has a strong narrow peak centered around 388 nm in the UV band, which can be attributed to the near-band-edge (NBE) transition of wide band gap ZnO nanowires arising from the recombination of free excitons through an exciton–exciton collision process [23]. A weak broad green band is also observed (Fig. 4 (inset)). Such emission has been attributed to deep-level defects (e.g. oxygen vacancy related shallow donors) originating in the ZnO crystals [23,24]. The high ratio of the UV to green emission intensities ($I_{UV}/I_G \approx 143$) indicates the good optical properties of these ZnO nanowires [25], which can be suitable candidates for optoelectronic devices [26].

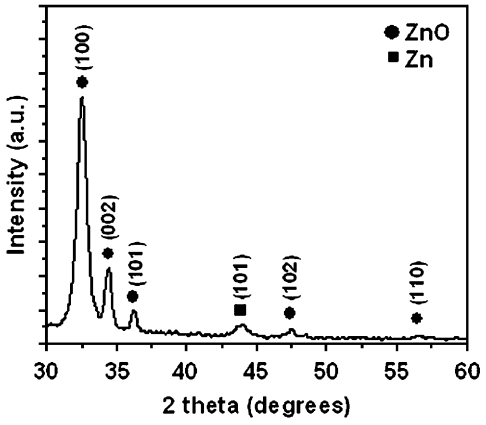

Fig. 3. XRD spectrum of the ZnO nanowires. There is a weak Zn (1 0 1) peak present, which could originate from incompletely transformed Zn in the interior of the particles.

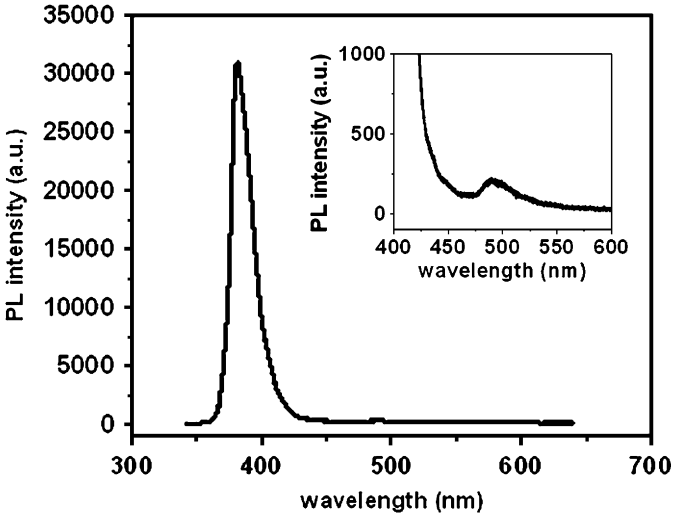

Fig. 4. Room temperature PL spectrum of the ZnO nanowires.

The microstructure of the ZnO nanowires was observed under TEM by direct growth of the nanowires onto a customized TEM silicon nitride grid with a hole at the center. With this arrangement, nanowires grow horizontally from the edge of the hole and can be examined with no interference from the support film. Bright-field images show that these nanowires have typical diameters of 5–20 nm (Fig. 5a). The inset of Fig. 5a is a magnified view of a typical nanowire tip and shows that the tip is clean and devoid of any foreign catalyst particles. Fig. 5b shows a high-resolution image (HRTEM) of a nanowire with the inset showing the selected area diffraction pattern from the same nanowire, revealing that the nanowire is single-crystalline. The diffraction pattern can be indexed as hexagonal wurtzite ZnO, with the zone axis deduced to be $[\bar{1}\,2\,\bar{1}\,3]$. The lattice spacing of 2.83 Å shown in Fig. 5b corresponds well to the known value of 2.81 Å for the $(1\,0\,\bar{1}\,0)$ planes of hexagonal ZnO with a direction at 30° to the growth direction of the nanowire. Of the three fast growth directions of ZnO, namely $\langle 2\,\bar{1}\,\bar{1}\,0\rangle$, $\langle 0\,1\,\bar{1}\,0\rangle$, and [0 0 0 1] [14], only $\langle 2\,\bar{1}\,\bar{1}\,0\rangle$ (*a*-axis) lies in the growth direction for our nanowires and is thus the most likely growth direction for our nanowire. More than 10 nanowires were examined by TEM and the growth directions deduced are consistent. A similar *a*-axis growth direction

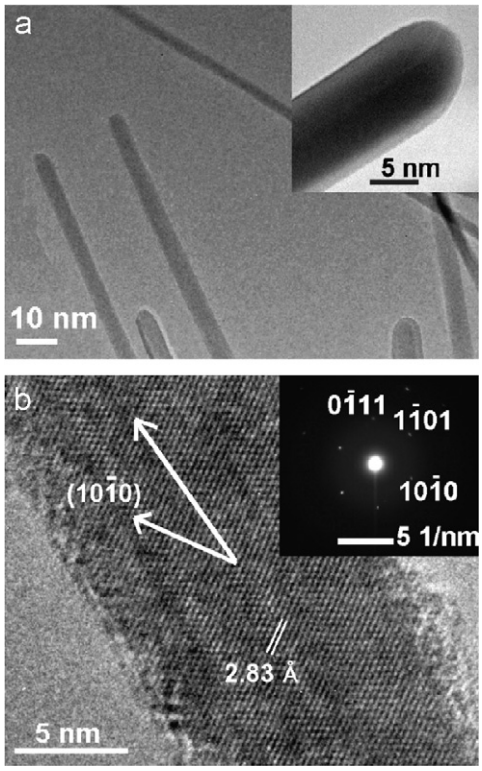

Fig. 5. TEM images showing (a) bright-field image of as-grown ZnO nanowires and the tip of a single nanowire (inset) and (b) HRTEM image and diffraction pattern (inset) of a single ZnO nanowire.

for ZnO nanowires has been reported recently, though under different growth conditions [15,16].

3.3. Nanowire growth mechanism

ZnO nanowires grown by the catalyst-assisted VLS growth mechanism normally have a catalyst nanoparticle embedded at their tips. However, no such foreign particles were found during TEM examination of our ZnO nanowire tips. Furthermore, we did not observe any nanowires growing on Au patterns, which had been fabricated adjacent to the patterned Zn on the same substrate. This excludes the catalyst-assisted VLS growth mechanism for the formation of ZnO nanowires in our experiment. On the other hand, though the exact mechanism responsible for ZnO one-dimensional growth in the VS growth process is still not clear [27,28], it is generally accepted that the control of supersaturation of the ZnO vapor is a prime consideration in obtaining the one-dimensional nanostructures. There are supporting pieces of evidence in the current literature that demonstrate that in the VS growth mode, the degree of supersaturation of the ZnO vapor determines the prevailing growth morphology of the ZnO crystal [27–31], and hence a low supersaturation of the ZnO vapor promotes whiskers or nanowires growth while a high supersaturation of the vapor causes large crystals to be formed. However, in our case, the same growth morphology, i.e., nanowires grow from a large patterned Zn region ($\sim 5 \times 5$ mm) as well as from a single Zn grain ($\sim$250 nm diameter) under the same growth conditions. A large patterned Zn region is expected to have a higher amount of local Zn vapor compared to the single Zn grain with respect to the same growth condition, and hence, the supersaturation of ZnO vapor is expected to be different in both cases, which will affect the nanostructure morphology if the VS growth mechanism is valid. Furthermore, it is also known that for the VS growth process, the morphology of the one-dimensional ZnO nanostructures synthesized changes (e.g. nanowires, nanobelts, nanosheets, etc.) with variations in the growth temperature and gas flow [30,31]. It is predicted that this change in growth morphology may be due to changes in the supersaturation of the ZnO vapor at different growth temperature and gas flow. In our case, we experimented with different growth temperature (500–700 °C) and gas flow ratio (oxygen/argon ratio) as reported in our previous works [26,32], but the same nanostructure morphology (i.e., nanowires) is obtained. Therefore, based on the above experimental evidences, we exclude the VS mechanism governing the growth of nanowires in our technique. Thus, the nature of the nanowire growth in our present technique suggests a different growth mechanism.

To elucidate how these nanowires emerged from the deposited Zn grains, we used some single Zn grains that were sparsely deposited onto a separate insulating substrate by the Ar sputtering pretreatment method for further investigations. It is difficult to perform such an investigation on patterned Zn regions that contain many densely packed grains. In addition, abutting grains inevitably fuse together when heated up to the growth temperature. During the experiment the morphology of a single Zn grain was observed in SEM. Fig. 6a depicts a typical Zn grain, which consists of a hexagonal-shaped base as shown from the top view. Side-view SEM images reveal two different morphologies: some grains have bases of the same size in a back-to-back configuration (Fig. 6b), while others have unequal sized bases (Fig. 6c). For both types of morphology, the edges of the grain appear thinner than the center.

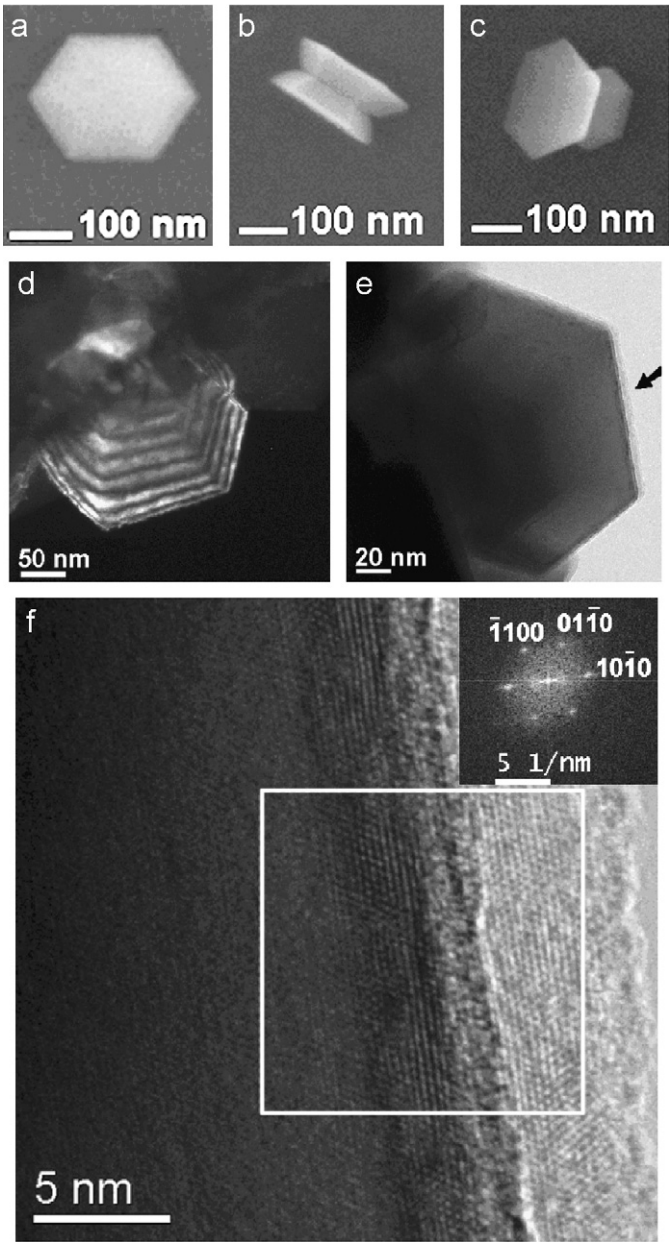

Fig. 6. As-deposited single Zn grains: (a) top view SEM image, (b) and (c) side view SEM images showing two different grain morphologies, (d) dark field TEM image, (e) bright field TEM image, and (f) HRTEM image at the grain edge and diffractogram (inset).

The microstructure of these Zn grains was analyzed by direct deposition of these grains onto a TEM copper grid before they were observed under the TEM. Fig. 6d shows a dark-field TEM image of a single grain showing thickness fringes. Such fringes appear at equal thickness intervals and their approximately uniform spacing suggests that the thickness increases linearly from the edge of the grain towards the center. This observation is in good agreement with the side-view SEM images of Figs. 6b, c and e which show a bright-field image of another grain of ~200 nm width whilst Fig. 6f shows an HRTEM from the edge of the grain marked by the arrow in Fig. 6e. At the region demarcated by the rectangle in Fig. 6f, a diffractogram was taken as shown in the inset of Fig. 6f. This diffractogram corresponds to an [0 0 0 1] single-crystal pattern of hexagonal Zn, showing that the top and bottom surfaces of the as-deposited grain are a pair of (0 0 0 1) and (0 0 0 $\bar{1}$) *c* planes, while the six side facets are {0 1 $\bar{1}$ 0}.

The sample with sparse grains was subjected to similar oxidation conditions as described above to grow the ZnO nanowires. SEM images reveal that the as-grown nanowires grow laterally from the edges of the single grain (Fig. 7a). Some grains also show preferential growth of the nanowires from the apices of the quasi-hexagonal-shaped grains (Fig. 7b). It was also observed that no nanowires grow from the top surface of the grain. Side view SEM images of the grains further reveal that these nanowires have grown in plane from the base of the grain (Figs. 7c and d). TEM imaging (not shown here) performed on these nanowires reveals that they are single-crystalline with a ZnO *a*-axis growth direction.

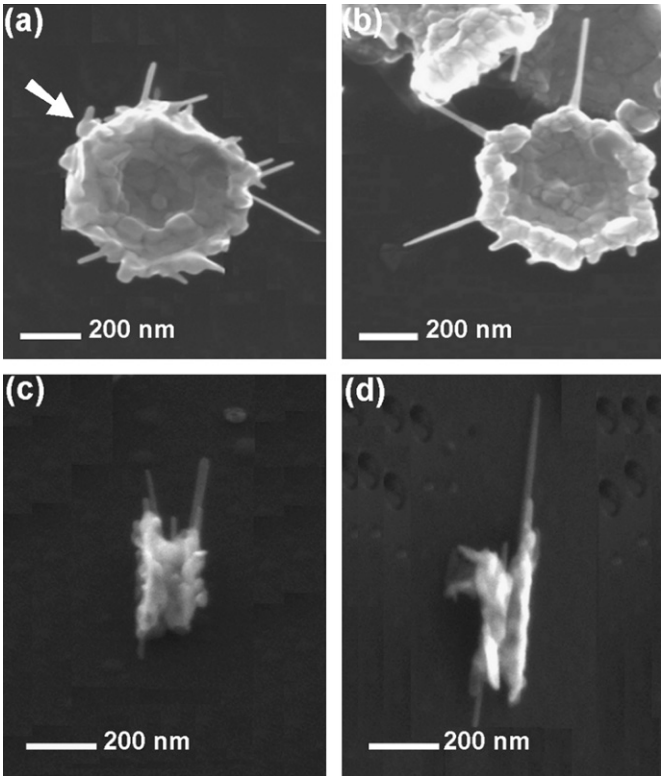

Fig. 7. SEM images of single Zn grains after oxidation showing nanowires grow laterally from the edges of the grain: (a) and (b) top view, (c) and (d) side view. The arrow in (a) indicates a nanocluster, which seeds the nanowire growth.

From our experiment, it is evident that the Zn grain not only functions as a seed layer for selective growth, but it also acts as a reactant and a catalyst (i.e., by providing an energetically favorable site for oxidation) simultaneously. In this sense, the growth process can be considered as "self-catalyzed" growth. We believe our growth process is similar in nature to previous reports of "self-catalyzed" growth of ZnO nanowires from metallic Zn by Dang et al. [33], Kim et al. [15] and Fan et al. [16], though no site-specific nanowire growth is demonstrated in these reports. Dang et al. [33] reported the synthesis of metal oxide nanowires by direct heating of the metal powder in appropriate oxygen atmospheres while Kim et al. [15] and Fan et al. [16] showed the formation of ZnO nanowires directly from physical-vapor deposited Zn plates and Zn polyhedrals via thermal oxidation in air.

The ZnO nanowires in our experiment grow laterally from the edges of the quasi-hexagonal-shaped grain. No nanowire growth from the top surface of the grain was observed. Similar nanowire growth behavior is also demonstrated by Kim et al. [15] and Fan et al. [16], but neither gives any discussion or reason for the lateral growth of nanowires from the edges of the Zn nanoplate or polyhedral. Kim et al. [15] suggested that the liquid phase Zn or ZnO_x formed at the apices of the Zn nanoplate acts as a nucleation site for the ZnO nanowire growth, but they did not elaborate why they are formed preferentially at the apices. Fan et al. [16] described briefly that the growth of the ZnO dendritic arms from the Zn polyhedral is due to a "self-catalytic" liquid–solid process in which the liquid Zn acts as both a reactant and a catalyst during the thermal oxidation process. For our case, we try to postulate the lateral growth of ZnO nanowires from the Zn grains in light of the SEM and TEM results obtained in our experiment in order to provide further insight into this similar growth technique.

Based on the above experiment showing the lateral growth of ZnO nanowires from single Zn grains, a growth mechanism is postulated as illustrated in the diagram shown in Fig. 8. When a hexagonal-shaped Zn grain (Fig. 8a) is subjected to a growth temperature of 500 °C, it will start to melt since the melting point of Zn is approximately 419 °C (Fig. 8b). From the microstructure characterization of the hexagonal Zn grain as observed in Fig. 6, it is possible that edge-enhanced oxidation effect of the grain coupled with the thermodynamic reaction between molten Zn and the surrounding oxygen in the air could result in the formation of ZnO nanoclusters at the edges of the grain (Fig. 8c). These reactions are elaborated as follows. It is generally known that the oxidation rates on different crystal surfaces are different—high-energy surfaces have enhanced oxidation compared to low energy surfaces which are more stable [34]. For the case of our

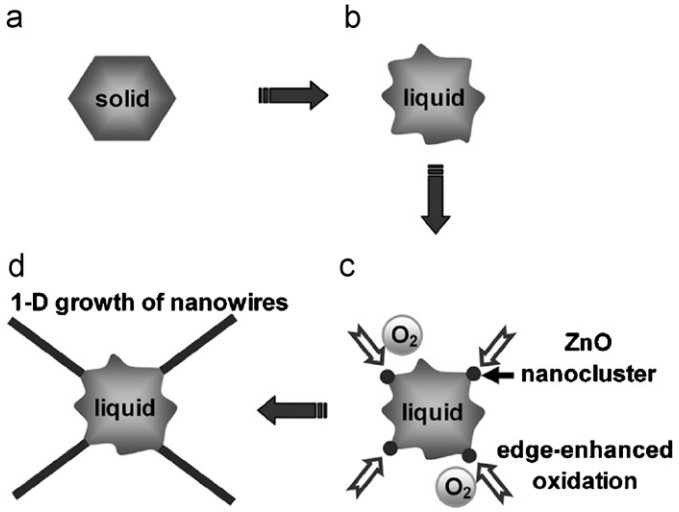

Fig. 8. Postulated nanowire growth mechanism.

hexagonal Zn grain, from the surface-energy perspective, the side/edge surfaces $\{0\,1\,\bar{1}\,0\}$ of Zn grain are known to have a higher energy surface than the top and bottom $\{0\,0\,0\,1\}$ surfaces [35]. This may result in preferential oxidation of the Zn grain at the edges (edge-enhanced oxidation effect) and could account for the preferential growth of nanowires from the grain edges rather than from the top surface as observed in the nanowires grown by our technique as well as similar growth technique reported in Refs. [15,16]. Experimental evidence to support the edge-enhanced oxidation effect of the Zn grains is shown in Ref. [29] where Gao et al. show enhanced oxidation at the edges of the Zn polyhedral than the top/bottom Zn grain surface to form ZnO. In addition, the thermodynamic reaction of the molten Zn with the surrounding oxygen in air forms solid ZnO, described by the following equation: $Zn(l)+O_2(g)\rightarrow ZnO(s)$. This reaction is expected to be spontaneous due to a negative Gibbs free energy [36]. The solid ZnO (nanoclusters) forms are estimated to be of nanometer sizes, as predicted by classical nucleation theory for a reaction between molten Zn with a low partial pressure of oxygen [37]. A low partial pressure of oxygen is expected in the vapor phase over the molten Zn due to the presence of Zn vapor (Zn has a high vapor pressure) at this growth temperature. These nanoclusters in turn act as nucleation sites for the preferential growth of the nanowires (Fig. 8d). This hypothesis can be corroborated by evidence shown in Fig. 7a, where the arrow indicates the presence of nanometer-scale cluster at the edge of the grain from which a nanowire emerges. We have viewed more than five SEM images of different grains showing similar nanoclusters from which a short nanowire grows. These evidences led us to assume that the nanclusters act as nucleation sites for the nanowire growth. Furthermore, solid ZnO is known to have poor wetting characteristics on molten Zn because the contact angle estimated using the equation of state and Young's equation is high [37]. Sharma and Sunkara [37] demonstrated that one-dimensional gallium oxide (GaO) nanowires rather than two-dimensional or three-dimensional crystals result from the oxidation of molten Ga due to a poor wettability of solid GaO on molten Ga. We believe the same mechanism is at play for our solid ZnO/molten Zn system. Poor wettability of the ZnO on molten Zn [37] causes the ZnO nanocluster nuclei to stay at the surface rather than agglomerate, and thus promote the one-dimensional growth of these nanowires. The growing nanowire then follows the template of the base Zn and grows in plane with the crystal. However, we do note that the above-proposed mechanism is speculative. Further experimental investigation, such as a real-time in situ TEM study of the self-catalyzed growth of ZnO nanowires directly from Zn grains by thermal oxidation, will be needed in order to elucidate the growth mechanism.

4. Conclusion

In summary, we have demonstrated a technique for site-specific growth of ZnO nanowires via a process, which is compatible with semiconductor processing. The as-synthesized nanowires are hexagonal-structured ZnO and are single-crystalline as revealed by XRD and electron microscopy. The room temperature PL spectrum of the nanowires shows a strong narrow UV emission band at 388 nm and a weak broad green band, indicating good optical properties. The growth mechanism is proposed to be due to a "self-catalyzed" growth from the metallic Zn grains. Coupled with edge-enhanced oxidation effect of the Zn grains and thermodynamic reaction between the molten Zn and the surrounding oxygen, ZnO nanoclusters are formed at the edges of the grain which seed the nanowire growth. Poor wettability of the ZnO on molten Zn promotes the one-dimensional growth of these nanowires. Understanding the unique growth behavior of these nanowires may pave the way for a more controlled growth of ZnO nanowires at site-specific locations on a substrate for the fabrication of planar ZnO nanowire devices.

Acknowledgments

The authors acknowledge A*STAR for funding support. We also thank H.Q. Le for help with the PL measurement. J.B.K. Law acknowledges A*STAR for a Graduate Scholarship Award.

References

[1] Y.W. Heo, D.P. Norton, L.C. Tien, Y. Kwon, B.S. Kang, F. Ren, S.J. Pearton, J.R. LaRoche, Mater. Sci. Eng. R 47 (2004) 1.
[2] Z.L. Wang, J. Phys. Condens. Matter 16 (2004) R829.
[3] G.-C. Yi, C. Wang, W.I. Park, Semicond. Sci. Technol. 20 (2005) S22.
[4] H.J. Fan, P. Werner, M. Zacharias, Small 2 (2006) 700.
[5] H. Cheng, J. Cheng, Y. Zhang, Q.-M. Wang, J. Crystal Growth 299 (2007) 34.
[6] M. Wang, C.H. Ye, Y. Zhang, G.M. Hua, H.X. Wang, M.G. Kong, L.D. Zhang, J. Crystal Growth 291 (2006) 334.

[7] X.D. Wang, C.J. Summers, Z.L. Wang, Nano Lett. 4 (2004) 423.
[8] M.H. Huang, S. Mao, H. Feick, H. Yan, Y. Wu, H. Kind, E. Weber, R. Russo, P. Yang, Science 292 (2001) 1897.
[9] H.J. Fan, W. Lee, R. Scholz, A. Dadgar, A. Krost, K. Nielsch, M. Zacharias, Nanotechnology 16 (2005) 913.
[10] E.C. Greyson, Y. Babayan, T.W. Odom, Adv. Mater. 16 (2004) 1348.
[11] J.J.F. Conley, L. Stecker, Y. Ono, Appl. Phys. Lett. 87 (2005) 223114.
[12] R.B.M. Cross, M.M. De Souza, E.M.S. Narayanan, Nanotechnology 16 (2005) 2188.
[13] M.-C. Jeong, B.-Y. Oh, O.-H. Nam, T. Kim, J.-M. Myoung, Nanotechnology 17 (2006) 526.
[14] H.T. Ng, J. Han, T. Yamada, P. Nguyen, Y.P. Chen, M. Meyyappan, Nano Lett. 4 (2004) 1247.
[15] T.-W. Kim, T. Kawazoe, S. Yamazaki, M. Ohtsu, T. Sekiguchi, Appl. Phys. Lett. 84 (2004) 3358.
[16] H.J. Fan, R. Scholz, F.M. Kolb, M. Zacharias, Appl. Phys. Lett. 85 (2004) 4142.
[17] J. Narayan, R.K. Venkatesan, A. Kvit, J. Nanopart. Res. 4 (2002) 265.
[18] L. Vitos, A.V. Ruban, H.L. Skriver, J. Kollar, Surf. Sci. 411 (1998) 186.
[19] S. Sanchez, C. Gui, M. Elwenspoek, J. Micromech. Microeng. 7 (1997) 111.
[20] J.F. Hamilton, P.C. Logel, J. Catal. 29 (1973) 253.
[21] M.E. Behrndt, J. Vac. Sci. Technol. 8 (1971) 724.
[22] J.A. Venables, L. Giordano, J.H. Harding, J. Phys. Condens. Matter 18 (2006) S411.
[23] Y.C. Kong, D.P. Yu, B. Zhang, W. Fang, S.Q. Feng, Appl. Phys. Lett. 78 (2001) 407.
[24] A.F. Kohan, G. Ceder, D. Morgan, C.G. Van de Walle, Phys. Rev. B 61 (2000) 15019.
[25] C. Li, G. Fang, Q. Fu, F. Su, G. Li, X. Wu, X. Zhao, J. Crystal Growth 292 (2006) 19.
[26] J.B.K. Law, J.T.L. Thong, Appl. Phys. Lett. 88 (2006) 1331141.
[27] Y. Xia, P. Yang, Y. Sun, Y. Wu, B. Mayers, B. Gates, Y. Yin, F. Kim, H. Yan, Adv. Mater. 15 (2003) 353.
[28] A. Umar, E.K. Suh, Y.B. Hahn, J. Phys. D 40 (2007) 3478.
[29] G.W. Sears, Acta Metall. 3 (1955) 361.
[30] C. Ye, X. Fang, Y. Hao, X. Teng, L. Zhang, J. Phys. Chem. B 109 (2005) 19758.
[31] B.D. Yao, Y.F. Chan, N. Wang, Appl. Phys. Lett. 81 (2002) 757.
[32] J.B.K. Law, J.T.L. Thong, Nanotechnology 18 (2007) 055601.
[33] H.Y. Dang, J. Wang, S.S. Fan, Nanotechnology 14 (2003) 738.
[34] P.X. Gao, Z.L. Wang, J. Am. Chem. Soc. 125 (2003) 11299.
[35] P.X. Gao, C.S. Lao, Y. Ding, Z.L. Wang, Adv. Funct. Mater. 16 (2006) 53.
[36] H.J.T. Ellingham, J. Soc. Chem. Ind. 63 (1944) 125.
[37] S. Sharma, M.K. Sunkara, J. Am. Chem. Soc. 124 (2002) 12288.